Front. Energy 2025, 19(2): 227–239
https://doi.org/10.1007/s11708-025-0991-7

RESEARCH ARTICLE

Bird skeleton-inspired 3D hollow diamond-enhanced PEG composite PCM for photothermal conversion and thermal management

Zihao Zhao[1], Xurui Feng[2], Daili Feng (✉)[1,3], Chengming Li (✉)[2,4], Yanhui Feng (✉)[1,3], Junjun Wei (✉)[2,4]

1 School of Energy and Environmental Engineering, University of Science and Technology Beijing, Beijing 100083, China
2 Institute for Advanced Materials and Technology, University of Science and Technology Beijing, Beijing 100083, China
3 Beijing Key Laboratory of Energy Conservation and Emission Reduction for Metallurgical Industry, University of Science and Technology Beijing, Beijing 100083, China
4 Shunde Graduate School, University of Science and Technology Beijing, Foshan 528399, China

Abstract The use of porous skeletons for encapsulating phase change materials (PCMs) is an effective approach to addressing issues such as leakage, low thermal conductivity, and poor photothermal conversion efficiency. Inspired by the hollow skeletal structure found in birds in nature, high-quality 3D interconnected hollow diamond foam (HDF) was fabricated using a series of processes, including microwave plasma chemical vapor deposition (CVD), laser perforation, and acid immersion. This HDF was then used as a scaffold to encapsulate PEG2000. The results demonstrate that HDF significantly reduces the supercooling degree and latent heat discrepancy of PEG2000. Compared to pure PEG2000, the thermal conductivity of the HDF/PEG increased by 378%, while its latent heat reached 111.48 J/g, accompanied by a photothermal conversion efficiency of up to 86.68%. The significant performance improvement is mainly attributed to the combination of the excellent properties of the diamond with the inherent advantages of the 3D interconnected structure in HDF, which creates a high-conductivity transport network inside. Moreover, the HDF/PEG composite extends the temperature cycling time of electronic components by 4 times for heating and 2.3 times for cooling, thereby prolonging the operational lifetime of electronic devices. HDF/PEG offers an integrated solution for solar energy collection, photothermal conversion, heat dissipation in electronic components, and thermal energy transfer/storage. This innovative approach provides innovative ideas for the design and fabrication of composite PCMs and has great application potential, such as solar energy utilization, thermal management, and thermal energy storage.

Keywords phase change materials (PCMs), porous diamond, photothermal conversion, thermal management

1 Introduction

In recent years, the rapid economic growth has led to a continuous increase in energy demand, making clean and renewable energy sources effective means to alleviate energy issues. However, due to factors such as natural environmental conditions, renewable energy sources often exhibit intermittent and fluctuating characteristics. Latent heat thermal energy storage technology based on phase change materials (PCMs), by utilizing energy flows during phase transitions, effectively addresses the time gap between supply and demand in renewable energy systems [1]. This technology plays a crucial role in overcoming key technical challenges in the development and utilization of new energy sources and has significant strategic importance in driving the transformation of energy production and utilization methods [2,3]. To date, latent heat storage has been widely applied in various fields, including photothermal conversion [4], industrial waste heat recovery [5], absorption refrigeration [6], building insulation [7], catalyst [8], and thermal

Received Nov. 15, 2024; accepted Jan. 15, 2025; online Mar. 20, 2025
Correspondences: Daili Feng, dlfeng@ustb.edu.cn;
Chengming Li, chengmli@mater.ustb.edu.cn;
Yanhui Feng, yhfeng@me.ustb.edu.cn;
Junjun Wei, weijj@ustb.edu.cn

Special Issue: Thermo-mechanical Energy Storage Technologies

protection [9]. Particularly, the stable temperature maintained during phase transitions makes PCMs ideal for thermal management applications, such as in electronic components like chips and batteries [10].

Among various PCMs, polyethylene glycol (PEG) has gained significant attention due to its high energy density, non-toxicity, low supercooling, good chemical stability, and environmental friendliness [11]. However, several properties of PEG limit its broader application and development. For instance, leakage during the phase change process and its low thermal conductivity hinder its use in electronic device heat dissipation. Additionally, pure PEG has a negligible light absorption capacity, resulting in low photothermal conversion efficiency, which limits its application in photothermal conversion. To address these issues, the encapsulation of PCMs using porous scaffolds has emerged as one of the most effective strategies for improving its performance. This approach is currently a hot research topic [12]. Among such materials, 3D porous materials such as metallic foams [13] and porous carbon [14–16] are considered promising candidates to significantly enhance the performance of PCMs due to their high thermal conductivity, large porosity, high specific surface area, and continuous structure.

For example, Zhou et al. [13] encapsulated paraffin wax and PEG using copper foam (CF) to enhance their thermal properties. The results showed that the thermal conductivity of the composite material was increased by 335% and 123%, compared to pure paraffin wax (0.26 W/(m·K)) and PEG (0.51 W/(m·K)), respectively. Photothermal conversion efficiency was also enhanced by 130% and 138%. Li et al. [15] developed a PEG-loaded porous carbon derived from waste rice husks. The results indicated that the developed PEG/CNR exhibited excellent heat storage performance (137.22 J/g) and enhanced solar photothermal conversion efficiency (a 54.7% increase), and a capability to delay the surface temperature rise of electronic devices (891 s). However, the increase in thermal conductivity was modest (~0.3 W/(m·K)). Luo et al. [17] encapsulated PEG with reduced graphene oxide (rGO), which resulted in a 50% enhancement in thermal conductivity (~0.39 W/(m·K)). Furthermore, they introduced polydopamine (PDA) as a coating for rGO, through a coupling effect, further improved the photothermal conversion efficiency of the rGO-based composite PCM. The final material achieved a photothermal conversion efficiency of 88.9%, 2.4% higher than that without PDA. Fan et al. [18] used carbon foam obtained from the carbonization of melamine as a skeleton to encapsulate PEG, resulting in a composite PCM with excellent thermal properties (177.3 J/g) and photothermal conversion performance (< 90%). To further enhance the thermal properties and photothermal conversion efficiency of PEG, Liu et al. [19] used carbonized melamine as a base skeleton and then incorporated Ag and CdS nanoparticles to enhance its performance. The final composite materials exhibited thermal conductivities of 0.5, 0.44, and 0.61 W/(m·K), representing increases of 150%, 120%, and 205%, respectively, compared to pure PEG, with the photothermal conversion efficiency reaching a maximum of 94.6%. Additionally, the material's ability to delay the temperature rise of electronic devices was extended by 141 s.

In summary, encapsulating PEG in porous skeletons can improve its thermal properties and its application capabilities in areas such as photothermal conversion and thermal management of electronic components. However, these studies have demonstrated that the enhancement in thermal conductivity still remains limited to around 200%, leaving significant room for improvement. High thermal conductivity is critical for enhancing the photothermal conversion and thermal management performance of PCMs [20,21]. A higher thermal conductivity allows the large amount of heat generated by the spectral absorption layer to quickly transfer to the PCM, which is beneficial for improving thermal response time and reducing heat storage duration. This also minimizes heat loss between the PCM and the environment during energy storage. Therefore, it is critical to develop carbon frameworks with superior performance to enhance the application efficiency of PCMs.

In this study, diamond, known for its excellent thermal conductivity and low thermal expansion coefficient [22], was selected as the primary carbon framework material. A CF-supported DF framework was fabricated using microwave plasma CVD (MPCVD). Inspired by the hollow, network-like skeletal structure in birds, which enhances oxygen storage and promotes respiratory efficiency, a hollow diamond foam (HDF) skeleton was fabricated by employing a "laser perforation-acid leaching" process to remove CF. This approach improves loading capacity and strengthens heat transfer. Finally, PEG2000 was incorporated into the HDF structure to form a composite PCM (HDF/PEG). The test results show that HDF/PEG exhibits superior thermal performance, photothermal conversion efficiency, and thermal management capabilities, overcoming the application limitations of PEG2000. These promising results indicate that HDF/PEG can serve as an effective thermal storage material in environmental thermal management systems and energy-saving applications, providing a novel method for preparing multifunctional composite PCMs.

2 Preparation and characterization of materials

2.1 Experimental materials

The CF (porosity 70%) used in this study was purchased

from Suzhou Jiashide Metal Foam Co., Ltd., China. The anhydrous ethanol (purity 99.5%, McLin) was obtained from Beijing Honghu United Chemical Products Co., Ltd., China, and the PEG (PEG2000, melting point 52–54 °C) was purchased from Shanghai Aladdin Biochemical Technology Co., Ltd.

2.2 Preparation method

The preparation method for DF is illustrated in Fig. 1(a). First, CF is used as the substrate after being etched with dilute hydrochloric acid (to remove the oxide layer) and cleaned through ultrasonic treatment. A titanium (Ti) layer is then deposited onto the CF via radio frequency (RF) magnetron sputtering, with a RF power of 180–220 W, chamber pressure of 0.5–1 kPa, Ar flow rate of 60–80 sccm), serving as an intermediate layer for diamond deposition (to address the lattice mismatch and thermal expansion coefficient differences between copper and diamond). Next, the Ti-coated CF is immersed in a diamond nanocrystal suspension in deionized water. The suspension is boiled and subjected to ultrasonic treatment for 10 min to promote diamond nucleation. The solution is then left to stand for 2 h to further promote heterogeneous nucleation of diamond.

After drying, diamond growth is performed using the microwave plasma MPCVD method at chamber pressure of 6–7 kPa and a temperature of 750–800 °C, resulting in the formation of DF. Detailed information regarding the deposition process and parameters for both Ti coating and diamond can be found in previous work [16].

To obtain HDF, laser perforation is performed on the DF (with a perforation density of 5–15 holes/mm^2), followed by acid etching to remove the CF. The sample is then cleaned and dried to obtain the final HDF product (Fig. 1(c)).

In nature, the skeletons of birds are characterized by numerous internal pores. This unique structure not only makes their skeletons lighter but also enhances respiratory efficiency by storing more oxygen to support flight. Inspired by this structure, HDF utilizes HDF as a porous skeleton, with the PCM acting as “air” within the structure, to improve thermal storage and heat transfer efficiency during heating and cooling cycles.

The preparation of the composite material follows the melt infiltration method, as shown in Fig. 1(b). First, the HDF is placed in a beaker containing an adequate amount of PEG2000, ensuring that the HDF is centered for uniform infiltration. Subsequently, the mixture is vacuum-composite for 6 h at 80 °C in a vacuum oven. This process results in the formation of the HDF/PEG composite, as shown in Fig. 1(c).

2.3 Characterization method

The morphology of the sample was characterized using scanning electron microscopy (SEM) (ZEISS GeminiSEM 300). The thermal stability was analyzed using thermogravimetric analysis (TGA) (NETZSCH STA 2500 STA2500A-0204-N), with a heating rate of 10 °C/min and a temperature range of 30–800 °C under a nitrogen atmosphere. The crystallographic characteristics

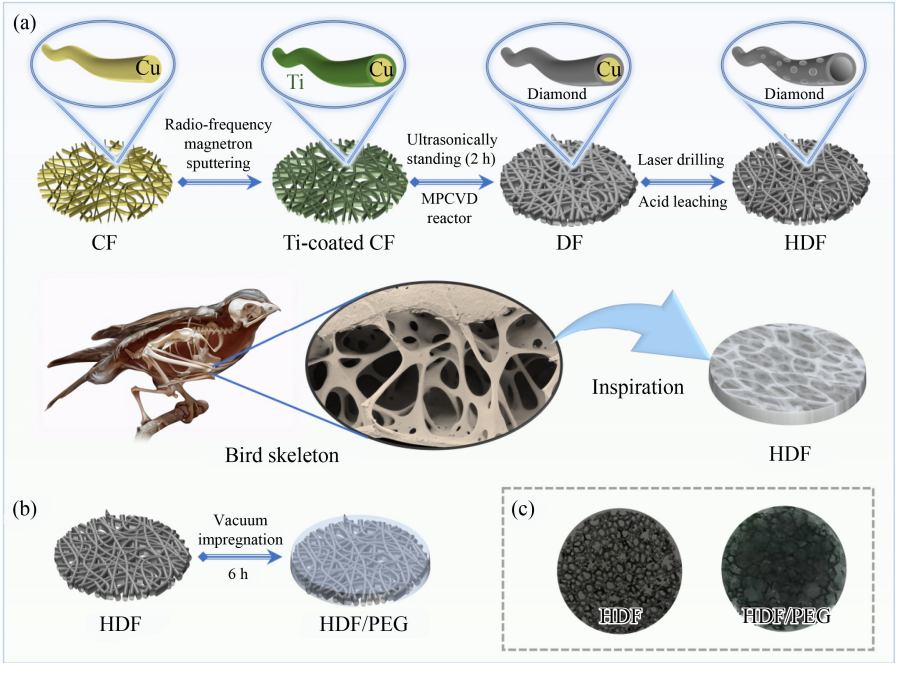

Fig. 1 Schematic diagram of material preparation process.
(a) Preparation of HDF skeleton; (b) preparation of HDF/PEG; (c) material picture: HAD (left), HAD/PEG (right).

of the samples were examined via X-ray diffraction (XRD) (Rigaku Ultima IV, Japan). The surface functional groups of HDF, PEG, and HDF/PEG were analyzed using Fourier transform infrared spectroscopy (FTIR) (Thermo Scientific Nicolet iS20). The quality of diamond growth on the surface was assessed with a high-resolution (HR) visible Raman spectrometer (Labram HR Ecolution), equipped with a charge-coupled device (CCD) and detector. The phase transition temperature, specific heat, and latent heat of phase transition were measured using differential scanning calorimetry (DSC), with nitrogen as the protective and purge gas. The DSC instrument used was METTLER DSC 3, with a sample mass of approximately 10 mg, a nitrogen flow rate of 50.0 mL/min, and a heating rate of 5 K/min. The thermal conductivity and specific heat of the materials were measured using the laser flash method (LFA) (NETZSCH LFA 457 MicroFlash), with each sample tested three times and error margin of ± 0.001–0.005 W/(m·K). The UV-visible-near-infrared (UV-vis-NIR) spectra of PEG2000 and the composite materials were recorded using a UV-Vis-NIR spectrophotometer (UV-3600 Plus) in the range of 200–2500 nm to assess the composite materials' absorption capacity for solar radiation.

The photothermal conversion performance of the materials was evaluated using a photothermal conversion test system, consisting of a xenon lamp light source (PLS-SXE300D, coupled with an AM 1.5G filter), a sample holder, and a multi-channel temperature recorder (YP5000). The sample holder and light source were placed in a sealed experimental chamber to minimize temperature loss and prevent interference from the external environment.

The heat management performance of the material for electronic components was tested using a custom experimental setup, mainly consisting of an alumina ceramic heating plate (20 mm × 20 mm), an infrared thermal imager (SC6X5-A615), and data acquisition equipment. Insulation materials were placed around the sample holder, and the entire setup was housed in a sealed experimental chamber to prevent interference from the external environment (See Table 1 for details).

3 Results and discussion

3.1 Morphology and structural characteristics

Figures 2(a)–2(b) show the microscopic morphology of the 3D HDF framework. In Fig. 2(a), a well-developed pore structure is observed, with distinct laser-drilled holes on the surface, and no copper is found inside the pores. The fracture morphology indicates that the framework is composed of a diamond film with a thickness of approximately 70–80 μm. Figure 2(b) reveals that the diamond film has a homogeneous and continuous structure, with diamond grains approximately 3–5 μm in size forming a typical "pyramid" structure, suggesting that the film has a microcrystalline nature, which enhances its heat transfer efficiency. The images in Figures 2(a)–2(b) confirm that the HDF is made of fully continuous diamond films without any gaps or cracks, forming a 3D continuous framework that ensures continuous heat conduction.

In addition to the continuous structure, the quality of the diamond films plays a crucial role in efficient heat transport. Figure 2(c) displays the Raman spectrum of the HDF, with a strong peak at 1331.98 cm^{-1}, which corresponds to the optimal quality of CVD-grown diamond [22]. This confirms that the quality of the HDF is exceptionally high, further supporting its potential for efficient thermal management.

FTIR spectra were used to further characterize the chemical structure and composition of PEG2000, HDF, and HDF/PEG composite (Fig. 2(d)). For PEG2000, distinct absorption peaks were observed at 961, 1100, 1360, 1472, 2884, and 3476 cm^{-1}. Specifically, the vibrations at 3436 cm^{-1} and 1100 cm^{-1} correspond to the

Table 1 Characterization device information

Characterization	Equipment	Model parameters
Morphology and structure	Scanning electron microscopy (SEM)	ZEISS GeminiSEM 300
	X-ray diffractometer (XRD)	Rigaku Ultima IV, Japan
	Fourier transform infrared spectroscopy (FT-IR)	Thermo Scientific Nicolet iS20
	Visible Raman spectrometer	Labram HR Ecolution
Thermal properties	Differential scanning calorimeter (DSC)	METTLER DSC 3
	Laser flash apparatus (LFA)	NETZSCH LFA 457 MicroFlash
	Thermogravimetric analysis (TGA)	NETZSCH STA 2500 STA2500A-0204-N
Application performance	UV-Vis-NIR Spectrophotometer	UV-3600 Plus
	Xenon lamp light source	PLS-SXE300D
	Multi-channel temperature recorder	YP5000
	Infrared thermal imager	SC6X5-A615

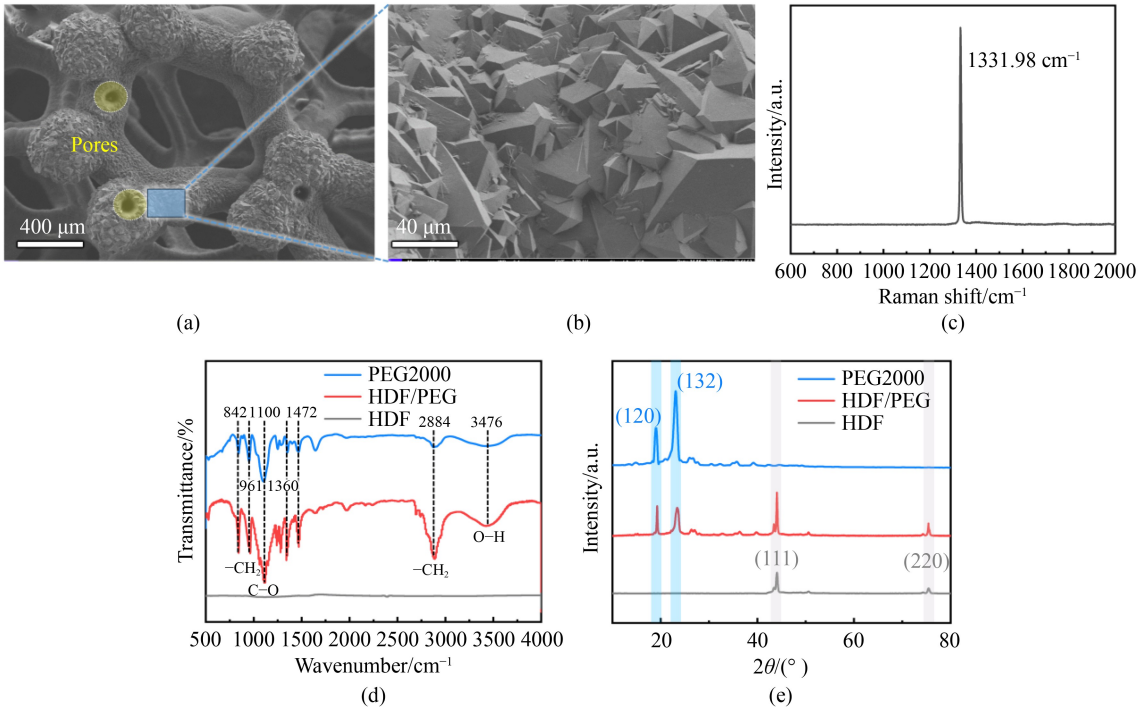

Fig. 2 Morphology and structural characteristics of HDF and HDF/PEG.
(a, b) SEM of the HDF; (c) Raman spectrum of the HDF; (d) FTIR spectra; (e) XRD patterns of PEG2000, HDF, and HDF/PEG.

stretching vibrations of the O–H and C–O bonds, respectively, while the vibrations at 2884 and 961 cm^{-1} are attributed to the stretching vibrations of the $–CH_2$ group [23]. In contrast, the FTIR spectrum of HDF does not show any distinct characteristic peaks. The FTIR spectrum of HDF/PEG, however, includes all the characteristic peaks of both the matrix and PCM, with no new absorption peaks or significant peak shifts. This confirms that PEG2000 and HDF interact primarily through physical bonding, without undergoing any chemical reactions.

FTIR analysis indicates that the adsorption and composite processes in the material result in only physical changes. To explore whether these processes affect the crystalline structure of PEG2000 and alter its phase change behavior and physical properties, X-ray diffraction (XRD) analysis was performed. The XRD patterns of PEG2000, HDF, and HDF/PEG are shown in Fig. 2(e). PEG2000 exhibits two strong, distinct characteristic peaks at 19.1° and 22.7°, corresponding to the (120) and (132) crystal planes [24], indicating good crystallinity. The XRD pattern of HDF shows two characteristic peaks at 43.8° and 75.7°, corresponding to the (111) and (120) planes of diamond, with no other significant impurity peaks. This confirms the high-quality diamond films and complete removal of CF [25].

For HDF/PEG composite, all the characteristic peaks of both HDF and PEG2000 are present, that confirming that PEG2000 undergoes a phase change process within HDF structure, generating latent heat. After the composite formation, slight changes in the peak width and intensity of PEG2000 were observed, which can be attributed to the confinement and wall effects of the porous structure of HDF structure on the PCM, influencing its phase change behavior [2].

3.2 Thermal properties

The heat storage performance of PEG2000 and HDF/PEG was tested using differential scanning calorimetry (DSC) (Figs. 3(a) and 3(b)). Both materials show similar trends, with clear endothermic and exothermic peaks. The melting latent heat and solidification latent heat of HDF/PEG are 111.48 and 111.31 J/g, respectively, which are lower than those of PEG2000 (152.06/139.45 J/g). This reduction can be attributed to the presence of HDF, which occupies some of the volume, thereby reducing the amount of PEG2000 in the composite material. Despite this reduction in latent heat, the encapsulation process effectively minimizes the latent heat difference of the PCM. After encapsulation, the latent heat difference decreases from 12.61 J/g for pure PEG2000 to just 0.17 J/g for the composite. This reduction in latent heat difference results in less energy loss during each melting and solidification cycle, making the composite PCMs more efficient for energy storage applications.

Moreover, the incorporation of HDF into PEG2000 helps lower the melting point and raise the freezing point to alleviate the supercooling of PEG2000, reducing the

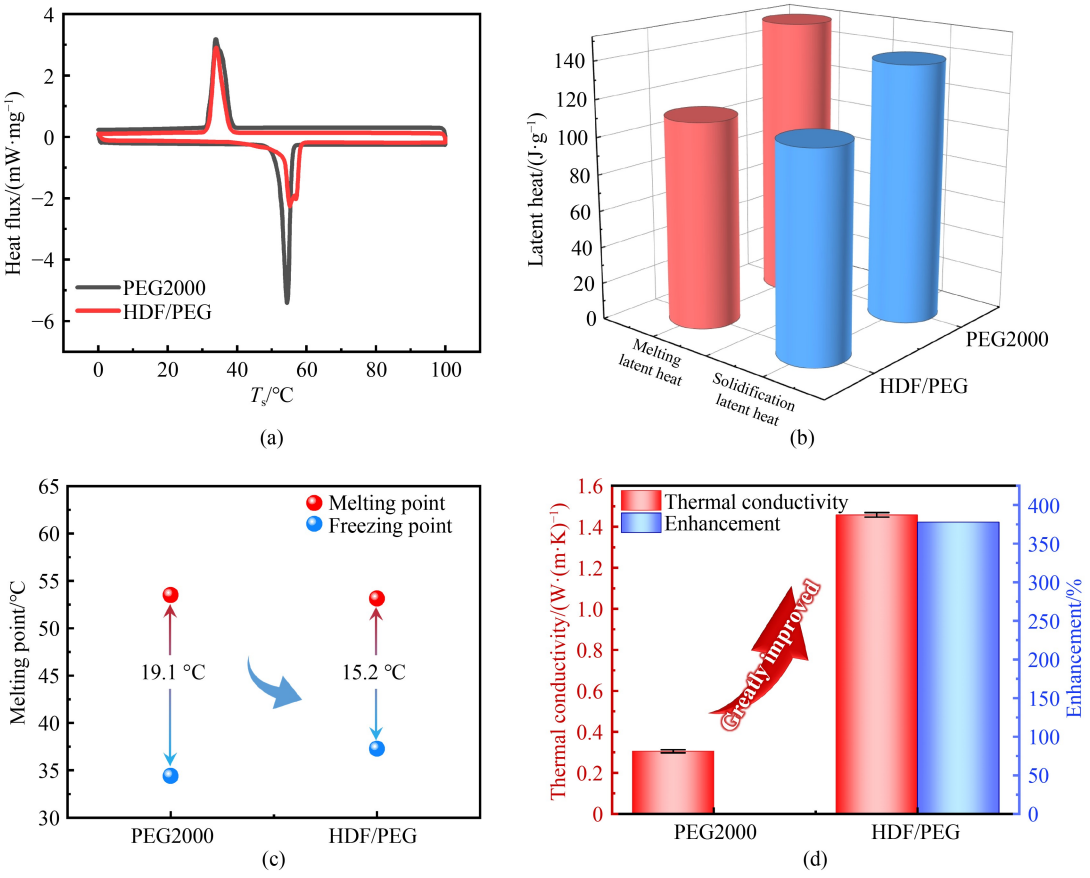

Fig. 3 Thermal characteristics of PEG2000 and HDF/PEG.
(a) DSC thermogram; (b) latent heat. (c) phase change point; (d) thermal conductivity.

degree of supercooling from 19.1 to 15.2 °C (Fig. 3(c)). This is because the thermally conductive network formed by the internal cross-linking of HDF accelerates heat transfer in PEG2000, thereby lowering the melting point. During solidification, HDF also accelerates heat dissipation and promotes nucleation, which in turn raises the freezing point and mitigates supercooling [15,26].

Thermal conductivity is a critical parameter for evaluating the performance of PCMs. The thermal conductivity of all samples was measured three times at room temperature, and the average value was recorded. The results, shown in Fig. 3(d), reveal that PEG2000 has a relatively low thermal conductivity of only 0.305 W/(m·K). In contrast, the thermal conductivity of the HDF/PEG composite reaches 1.458 W/(m·K), an improvement of 378%. This significant enhancement indicates that the 3D network structure within HDF provides effective thermal conduction pathways, greatly enhancing the heat transfer efficiency of the PCM (See Table 2 for detailed information on thermal characteristics).

3.3 Thermal stability

Thermal stability is crucial for the practical application of PCMs. The thermal stability of the materials was assessed through thermogravimetric experiments, with the results shown in Figs. 4(a) and 4(b). For PEG2000, the thermogravimetric curve remains flat with minimal changes up to 330 °C, indicating good thermal stability. However, after 320 °C, the curve shows a more significant change, and complete degradation occurs around 440 °C. In contrast, the weight loss of HDF/PEG mainly occurs in the temperature range of 320–420 °C,

Table 2 Thermal performance of PEG2000 and HDF/PEG2000

Sample	C_p/(J·(g·K)$^{-1}$)	(ΔH_m/ΔH_c)/(J·g^{-1})	ΔH/(J·g^{-1})	(T_m/T_c)/°C	T_{sc}/°C	k/(W·(m·K)$^{-1}$)	η/%
PEG2000	1.941	152.06/139.45	12.61	53.51/34.41	19.1	0.305	–
HDF/PEG2000	1.743	111.48/111.31	0.17	53.13/37.28	15.2	1.458	378

Note: C_p: specific heat; ΔH_m: melting latent heat; ΔH_c: latent heat of solidification; ΔH: latent heat difference; T_m: melting temperature; T_c: solidification temperature; T_{sc}: supercooling; k: thermal conductivity; η: enhancement of thermal conductivity.

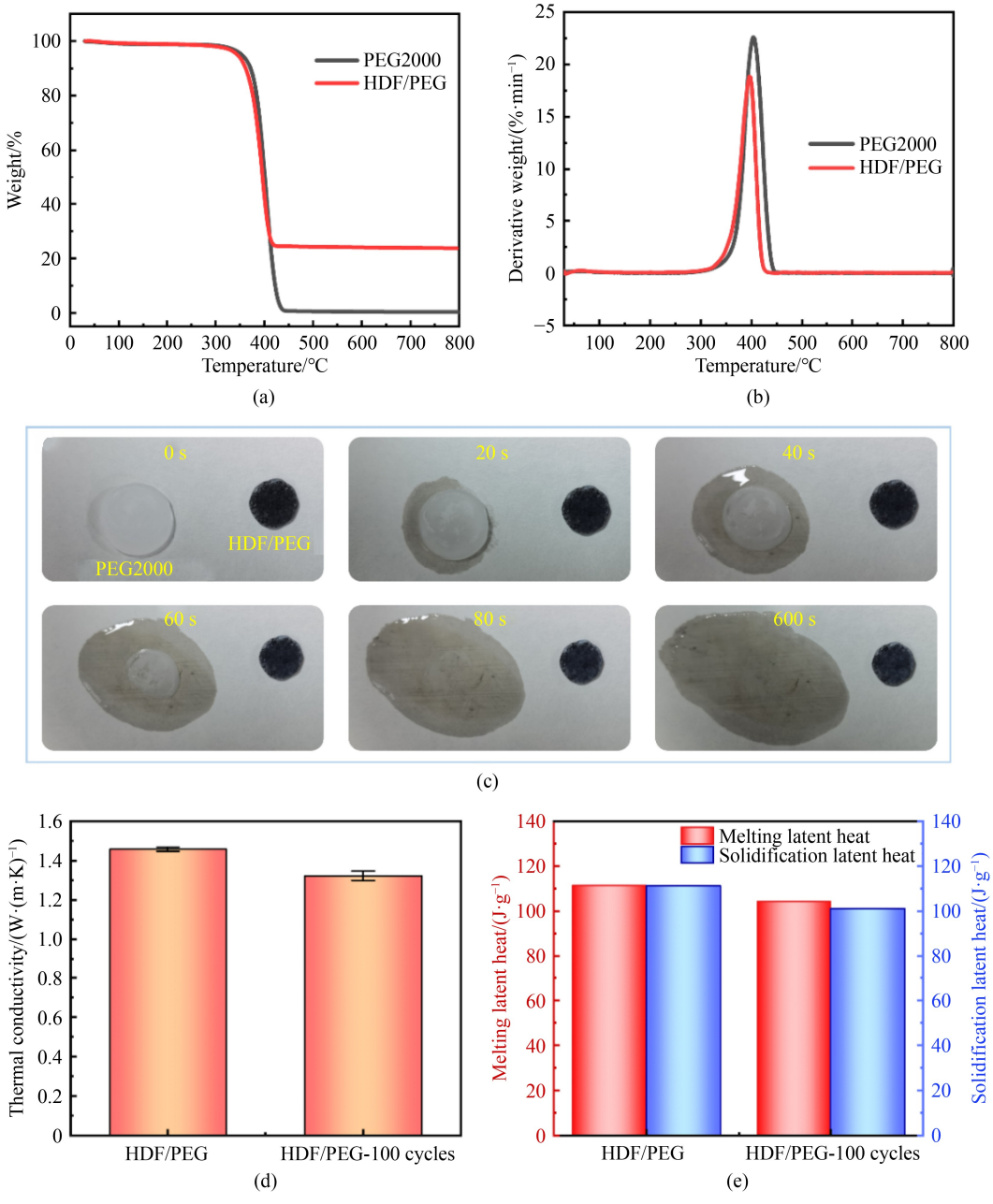

Fig. 4 Thermal and shape stability of HDF/PEG.

(a) TG curve of PEG2000 and HDF/PEG; (b) DTG curve of PEG2000 and HDF/PEG; (c) leakage test; (d, e) performance of HDF/PEG before and after cycling.

with minimal changes above 320 °C, indicating that the composite material maintains excellent thermal stability in the mid-to-low temperature range.

The thermogravimetric analysis also reveals that the theoretical encapsulation rate of HDF/PEG is 79%, suggesting that HDF has a good loading capacity for PEG2000. It can be observed that the decomposition rate of HDF/PEG is faster than that of PEG2000. This can be attributed to the high thermal conductivity of HDF, which enhances heat transfer and accelerates the degradation of the material. As shown in Fig. 4(b), before 400 °C, the decomposition rate of the composite material is significantly higher than that of PEG2000, and the peak width of the DTG curve is narrower, supporting this observation. After the complete degradation of PEG2000 in HDF/PEG composite, the remaining HDF framework maintains excellent thermal stability up to 800 °C.

The anti-leakage performance of PCM is a critical factor for evaluating their practicality in thermal energy storage applications. The leakage prevention capability of HDF for PEG2000 was tested by heating on a 70 °C hot plate, as shown in Fig. 4(c). The results show that

PEG2000 leaked significantly within 20 s and completely melted within 80 s. In contrast, the HDF/PEG composite remained stable throughout the heating process with no leakage observed, and no changes were detected even after ten minutes. This indicates that HDF provides excellent encapsulation, effectively preventing leakage of PEG2000. In addition, after undergoing 100 heating-cooling cycles (Figs. 4(d) and 4(e)), the thermal properties of the composite PCM remained stable, with less than a 10% change in performance, demonstrating that the material has good cycle stability.

3.4 Photothermal conversion

Solar radiation is characterized by intermittency and discontinuity, which presents challenges for energy conversion. However, the use of composite PCMs can effectively address the mismatch between solar radiation in both time and space [27,28]. To evaluate the spectral absorption capability of the materials, a UV-Vis-NIR spectrometer was employed, and the results are shown in Fig. 5(c). The composite materials exhibit higher spectral absorption in the visible light range, with a significant improvement compared to PEG2000, confirming that HDF enhances the solar energy absorption capacity of PEG2000.

The photothermal conversion capability of HAD/PEG was tested using a photothermal conversion experimental setup, as illustrated in Fig. 5(a). A Xenon lamp was used to simulate the solar light source with a power density of 0.6 W/cm^2, and the temperatures on both the top and bottom surfaces of the material were recorded. To more clearly observe the phase change process, the temperature on the bottom surface of the material (T_{bottom}) was primarily recorded, as shown in Fig. 5(b). Under Xenon lamp irradiation, the temperature on the bottom surface increased rapidly, indicating that the sample effectively captured solar energy. As the temperature continued to increase, a distinct “phase change plateau” appeared, signaling that PEG2000 was undergoing melting. During this phase, solar energy is converted into heat, which was rapidly transferred through the high thermal conductivity skeleton, thereby heating the PEG2000 molecules and driving the phase change process for photothermal conversion. Once PEG2000 was completely melted, the temperature continued to rise and reached a maximum of 54.5 °C within 5 min. During the cooling phase (after the light source was removed), the temperature dropped quickly, and once it reached the phase change temperature, it began to stabilize. A “phase change plateau” appeared, indicating that the stored solar energy was being released. The photothermal conversion efficiency of HAD/PEG was further calculated, using the expression

$$\eta = (m \cdot \Delta H)/(P \cdot S \cdot (t_e - t_0)) \times 100\%,$$

where η is the photothermal conversion efficiency of HDF/PEG; m is the mass of HDF/PEG, g; ΔH is the latent heat of the HDF/PEG, J/g; P is optical power density, W/cm^2; S is the illuminated area, cm^2; and t_0 and t_e are the start and end times of the phase transition, s.

The calculated photothermal conversion efficiency of HDF/PEG is 85.6%, as shown in Fig. 5(d). When compared to other composite PCMs with photothermal conversion capabilities reported in the literature [15,27–39], this material demonstrates superior photothermal conversion efficiency in terms of both photothermal conversion efficiency and heat storage capacity (See Table 3). These outstanding results highlight the potential of HDF/PEG materials for practical applications in solar thermal energy conversion, offering an effective solution to harness and store solar energy efficiently.

3.5 Thermal management of electronic components

For electronic devices, the miniaturization and high integration of chips may lead to transient temperature rise and uneven temperature distribution during operation, resulting in thermal and mechanical stresses that can cause device failure. The integration of PCMs (such as HDF/PEG) with electronic components can play a significant role in stabilizing the temperature of electronic devices, effectively preventing rapid temperature increases and mitigating thermal stresses that could lead to device failure during the operation of electronic components [40]. The thermal delay performance of HDF/PEG during heating and cooling cycles for electronic components was investigated, as shown in the experimental setup in Fig. 6(a). The setup involves an alumina ceramic heating plate (20 mm × 20 mm) which simulates chip heating by varying voltage levels (1, 2, and 3 V) while keeping a constant current (0.6 A) to simulate different operating conditions. A composite PCM sample (such as HDF/PEG) is placed above the heating plate, and thermal silicone grease is used to fill the gap between the PCM and the heating plate to eliminate the impact of air on heat conduction. K-type thin-film thermocouples are placed between the heating plate and the composite PCM to monitor the temperature variation (T_{surface}) on the upper surface of the heating plate during the heating and cooling phase. Additionally, infrared thermography is used to visually capture the temperature changes on the upper surface of both the heating plate and the composite material. Insulation materials are placed around the heating plate and sample to minimize the impact of ambient environmental changes on the measurements.

During the test, the initial temperature was set at 25 °C. The power supply was turned off when the temperature of the upper surface of the heating plate reached 75 °C, and recording ceased once the temperature cooled down

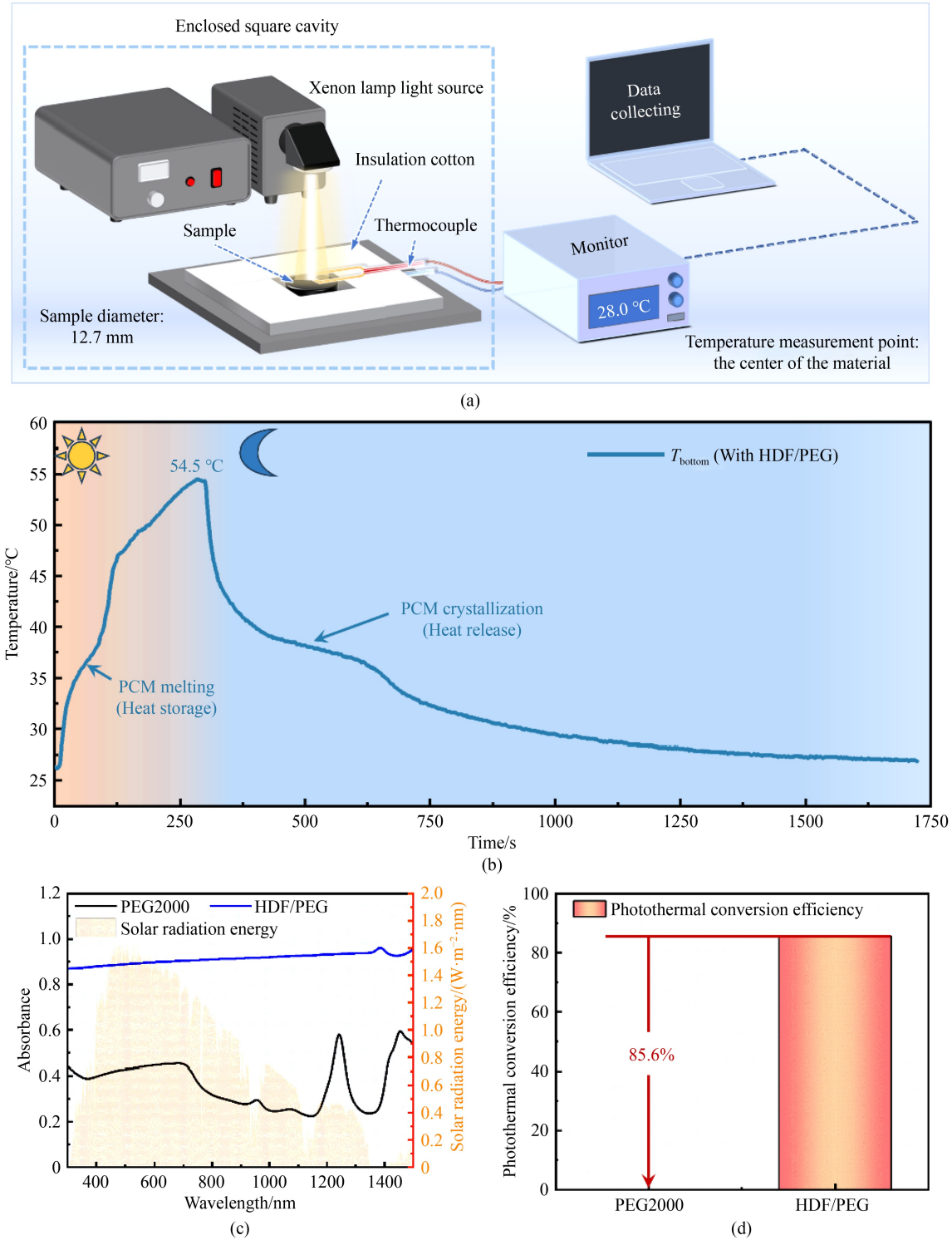

Fig. 5 Photothermal conversion characteristics of HDF/PEG.

(a) Schematic diagram of photothermal conversion experiment; (b) temperature–time response curve of photothermal conversion for HDF/PEG; (c) UV-visible-near-infrared absorption spectra of PEG2000 and HDF/PEG; (d) photothermal conversion efficiency.

to 25 °C. Figure 6(b) presents infrared thermal images of ceramic heating plates with and without the addition of HDF/PEG under voltages of 1, 2, and 3 V. It is evident that, compared to the rapid increase in surface temperature of the heating element without HDF/PEG, the temperature of the heating element coated with HDF/PEG is significantly constrained, which helps ensure the normal operation of the electronic device.

Table 3 Comparison of thermal conductivity, latent heat, and photo-thermal conversion properties of composite PCMs

Sample	Thermal conductivity/(W·(m·K)$^{-1}$)	($\Delta H_m/\Delta H_c$)/(J·g^{-1})	η/%	Ref.
PEG/CNR	–	137.22/132.57	54.7	Li et al. [15]
70 wt% PA/F-CuS	0.304	199.1/184.2	70.3	Yan et al. [27]
CF/(HO-BNNS@CuO)/PEG	1.12	152.3/146.8	91.8	Yang et al. [29]
MNH/CW	0.41	87.2/85.6	83	Zhang et al. [30]
SA/HS/TaON/SiW_{12}	0.483	126.4/115.9	80.5	Yan and Li [28]
B-GA-PCM	1.07	148.4/141.6	89.3	Bao et al. [31]
PRPf(9.5)	0.76	138.6/130.8	93.3	Yang et al. [32]
70% EG/OP70	1.413	126.7/126.9	58.2	Zou and Liu [33]
S5	2.2	145.4/144.6	72	Cai et al. [34]
OP70/EG	2.08	139.0/139.0	70	Chen et al. [35]
NPT-PCMs1	10.54	150.0/149.7	60.1	Luo et al. [36]
10% EG/PCM	6.01	215.7	81.9	Bai et al. [37]
PCM1(EG/SA)	11.71	159.36/159.58	95.3	Gao et al. [38]
18 wt%EG-OC	2.90	366.8	75.11	Huo et al. [39]
HDF/PEG	1.458	111.48/111.31	86.5	This work

Notes: ΔH_m: melting latent heat; ΔH_c: latent heat of solidification; η: photothermal conversion efficiency.

Figure 6(c) and Table 4 indicate that, without the composite PCMs, the surface temperature ($T_{surface}$) quickly rises from the initial 25 °C to the peak temperature of 75 °C. The heating rate increases with higher applied voltages. When HDF/PEG is applied, the heat generated during the initial heating phase is absorbed by the material. Although HDF/PEG can delay the temperature rise, its effect is limited during the early stages. As time progresses, the HDF/PEG begins to melt, converting heat into latent heat (manifested by a melting plateau) for storage, and the temperature rise delay effect becomes more pronounced. For example, at 1 V, $T_{surface}$ reaches 75 °C at 1441 s, indicating that the presence of HDF/PEG delayed the peak temperature by approximately twice the time compared to the heating element without the PCM. When the voltage is increased to 2 and 3 V, the delay becomes roughly 4 times longer.

During cooling, the surface temperature ($T_{surface}$) of the component without composite PCMs dropped rapidly. However, with HDF/PEG applied, the heat release from the electronic component occurred more slowly. Once the temperature reached the freezing point, the composite PCMs released the stored heat back into the component (manifested as a solidification plateau), preventing a sudden temperature drop. As an example, at 1 V, the electronic component coated with HDF/PEG takes 2418 s to cool to 25 °C, which is 2.3 times longer than the 1080 s it takes for the component without PCM coverage.

The use of composite PCMs significantly extends the heating/cooling cycle of the electronic component, alleviating thermal-mechanical cyclic fatigue inside electronic devices during real-world applications, thereby improving device stability. This makes HDF/PEG a promising material for thermal management of electronic devices.

4 Conclusions

This study innovatively combines natural design inspiration with advanced material science to create an efficient composite material for thermal management and energy storage. Drawing from the hollow, lattice-like skeletal structure of birds, which is optimized for oxygen storage and respiratory efficiency, the study uses CF as a template, titanium as an intermediate layer, and diamond films grown via microwave plasma CVD. The use of laser perforation and acid etching successfully removes the CF, resulting in a 3D continuous interconnected HDF.

Upon loading with PEG2000, a composite PCM, HDF/PEG, is obtained. Thanks to the high thermal conductivity network channels inside the 3D interconnected structure of HDF, the thermal conductivity of HDF/PEG reaches 1.458 W/(m·K), which is a 378% improvement compared to PEG2000 alone. Despite this improvement in thermal conductivity, the HDF/PEG maintains a high latent heat (111.48 J/g), which is crucial for efficient thermal energy storage, while reducing supercooling (decrease 26%) and latent heat difference (decrease 98.6%). The introduction of HDF also enhances the absorption of solar spectrum by PEG2000, resulting in a photothermal conversion efficiency of the composite material reaching 86.5%. Moreover, under low power, the HDF/PEG coverage can delay the heating and cooling cycles of electronic components by 4 and 2.3 times, respectively, thereby

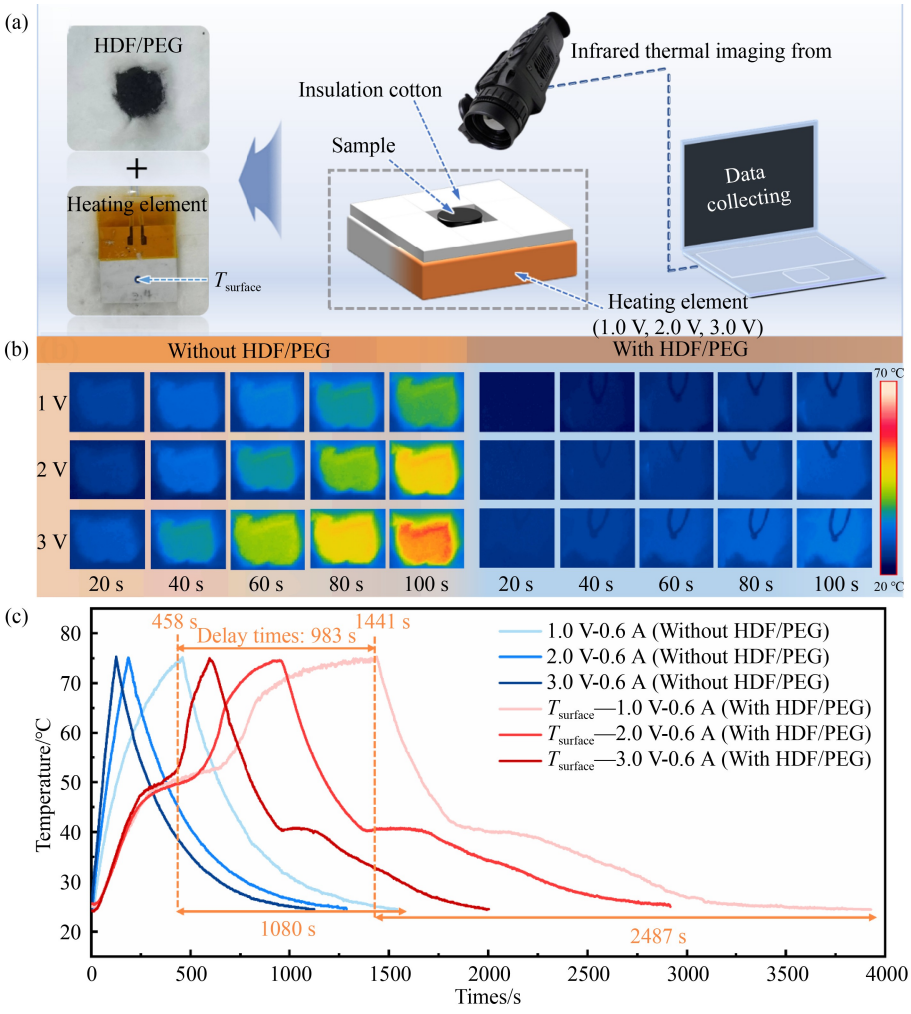

Fig. 6 Thermal management of electronic components.
(a) Schematic diagram of the thermal management experiment for electronic components; (b) infrared thermography of the thermal management experiment; (c) temperature–time response curve of the thermal management experiment.

Table 4 Comparison of temperature rise and fall time on electronic component surface with and without HDF/PEG

Sample	Voltage/V	$t_{heating}$/s	$t_{cooling}$/s
Without HDF/PEG	1.0	458	1080
	2.0	186	1099
	3.0	127	992
With HDF/PEG	1.0	1441	2487
	2.0	959	1964
	3.0	598	1404

Note: $t_{heating}$: time required for the component surface temperature to reach 75 °C; $t_{cooling}$: time required for the component surface temperature to drop from 75 to 25 °C.

extending the operating lifetime of the electronic components. The HDF/PEG composite integrates solar energy collection, photothermal conversion, heat dissipation for electronic components, and thermal energy transfer/storage. These results demonstrate the significant potential of HDF and its composites in the fundamental research and practical applications of efficient thermal management and thermal energy storage.

Acknowledgements This work was supported by the National Natural Science Foundation of China (Grant Nos. 52176054, 52236006, 52172037, and 52350362), the Natural Science Foundation of Guangdong Province, China (Grant No. 2024A1515012033).

Competing Interests The authors declare that they have no competing interests.

References

1. Gao H, Wang J, Chen X, et al. Nanoconfinement effects on thermal properties of nanoporous shape-stabilized composite PCMs: A review. Nano Energy, 2018, 53: 769–797
2. Feng D, Zhao Z, Li P, et al. Multifunctional performance of carbon nanotubes in thermal energy storage materials. Materials Today, 2024, 75: 285–308

3. Feng D, Zhao Z, Zhang X, et al. Carbon-based nanoadditives induced enhancement of phase change thermal properties of sugar alcohol and interfacial heat transport mechanisms. Composites Science and Technology, 2023, 243: 110258
4. Kong X, Liu X, Yuan J, et al. Composite phase change materials with thermal-flexible and efficient photothermal conversion properties for solar thermal management. Journal of Energy Storage, 2024, 78: 110027
5. Wi S, Jeong S G, Chang S J, et al. Evaluation of energy efficient hybrid hollow plaster panel using phase change material/xGnP composites. Applied Energy, 2017, 205: 1548–1559
6. Agyenim F, Eames P, Smyth M. Experimental study on the melting and solidification behaviour of a medium temperature phase change storage material (erythritol) system augmented with fins to power a LiBr/H_2O absorption cooling system. Renewable Energy, 2011, 36(1): 108–117
7. Yang H, Wang Y, Yu Q, et al. Composite phase change materials with good reversible thermochromic ability in delignified wood substrate for thermal energy storage. Applied Energy, 2018, 212: 455–464
8. Wang C, Ouyang Y, Luo Y, et al. Review on recent advances in phase change materials for enhancing the catalytic process. Chinese Journal of Catalysis, 2024, 60: 128–157
9. Geng X, Li W, Wang Y, et al. Reversible thermochromic microencapsulated phase change materials for thermal energy storage application in thermal protective clothing. Applied Energy, 2018, 217: 281–294
10. Kong X, Nie R, Yuan J. Shape stabilized three-dimensional porous SiC-based phase change materials for thermal management of electronic components. Chemical Engineering Journal, 2023, 462: 142168
11. Feng D, Li P, Feng Y, et al. Using mesoporous carbon to pack polyethylene glycol as a shape-stabilized phase change material with excellent energy storage capacity and thermal conductivity. Microporous and Mesoporous Materials, 2021, 310: 110631
12. Li P, Feng D, Feng Y, et al. Thermal properties of PEG/MOF-5 regularized nanoporous composite phase change materials: A molecular dynamics simulation. Case Studies in Thermal Engineering, 2021, 26: 101027
13. Zhou M, Tan Y, Chen R, et al. Erythritol supported by carbon nanotubes reinforced alumina-silica aerogels as novel form-stable phase change materials with high photothermal conversion efficiency and greatly suppressed supercooling. Journal of Energy Storage, 2024, 90: 111909
14. Li S Y, Yan T, Huo Y J, et al. Polydopamine/copper nanoparticles synergistically modified carbon foam/octadecanol composite phase change materials for photothermal energy conversion and storage. Chemical Engineering Science, 2024, 300: 120601
15. Li P, Feng D, Feng Y, et al. Converting bio-waste rice into ultralight hierarchical porous carbon to pack polyethylene glycol for multifunctional applications: Experiment and molecular dynamics simulations. Composites. Part A, Applied Science and Manufacturing, 2024, 178: 107979
16. Feng X, Zhang Y, Yang Z, et al. Polyethylene glycol with dual three-dimensional porous carbon nanotube/diamond: A high thermal conductivity of composite PCM. Nanotechnology, 2024, 35(9): 095702
17. Luo W, Zou M, Luo L, et al. Efficient enhancement of photothermal conversion of polymer-coated phase change materials based on reduced graphene oxide and polyethylene glycol. Journal of Energy Storage, 2024, 78: 109950
18. Fan R, Zheng N, Sun Z. Enhanced photothermal conversion capability of melamine foam-derived carbon foam-based form-stable phase change composites. Energy Conversion and Management, 2022, 263: 115693
19. Liu Y, Liu Y, Chen W, et al. Polyethylene glycol/melamine foam composite phase change materials modified by CdS/Ag exhibits high photothermal conversion performance. Desalination, 2024, 585: 117783
20. Li T, Wu M, Wu S, et al. Highly conductive phase change composites enabled by vertically-aligned reticulated graphite nanoplatelets for high-temperature solar photo/electro-thermal energy conversion, harvesting and storage. Nano Energy, 2021, 89: 106338
21. Zhang W, Ling Z, Fang X, et al. Anisotropically conductive $Mg(NO_3)_26H_2O$/g-C_3N_4-graphite sheet phase change material for enhanced photo-thermal storage. Chemical Engineering Journal, 2022, 430: 132997
22. Zhang L, Zhou K, Wei Q, et al. Thermal conductivity enhancement of phase change materials with 3D porous diamond foam for thermal energy storage. Applied Energy, 2019, 233–234: 208–219
23. Cheng M, Hu J, Xia J, et al. One-step *in-situ* green synthesis of cellulose nanocrystal aerogel based shape stable phase change material. Chemical Engineering Journal, 2022, 431: 133935
24. Zheng C, Zhang H, Xu L, et al. Carbonized bamboo parenchyma cells loaded with functional carbon nanotubes for preparation composite phase change materials with superior thermal conductivity and photo-thermal conversion efficiency. Journal of Building Engineering, 2022, 56: 104749
25. Shao W, Ivanov V, Zhen L, et al. A study on graphitization of diamond in copper–diamond composite materials. Materials Letters, 2004, 58(1–2): 146–149
26. Atinafu D G, Chang S J, Kim K H, et al. A novel enhancement of shape/thermal stability and energy-storage capacity of phase change materials through the formation of composites with 3D porous (3,6)-connected metal–organic framework. Chemical Engineering Journal, 2020, 389: 124430
27. Yan T, Chang X L, Huo Y J, et al. Preparation and characteristic of palmitic acid/flower-shaped CuS composite phase change material for effective heat storage and photothermal conversion. Materials Today Sustainability, 2024, 26: 100768
28. Yan D, Li M. Stearic acid-modified MOF-based composite phase change materials for solar-thermal energy conversion and storage. Solar Energy, 2023, 262: 111843
29. Yang H, He L, Liu R, et al. Ultralight and flexible carbon-based phase change composites with high porosity for enhanced shape memory and photothermal conversion performance. Solar Energy Materials and Solar Cells, 2022, 244: 111816
30. Zhang H, Ling Z, Zhou S, et al. Preparation and characteristic of wood-based inorganic composite phase change material with

effective anisotropic thermal conductivity for thermal energy storage. Solar Energy Materials and Solar Cells, 2023, 251: 112172

31. Bao Z, Bing N, Yao H, et al. Three-dimensional interpenetrating network phase-change composites with high photothermal conversion and rapid heat storage and release. ACS Applied Energy Materials, 2021, 4(8): 7710–7720
32. Yang H, Bai Y, Ge C, et al. Polyethylene glycol-based phase change materials with high photothermal conversion efficiency and shape stability in an aqueous environment for solar water heater. Composites. Part A, Applied Science and Manufacturing, 2022, 154: 106778
33. Zou X, Liu J. Polyoxyethylene based phase change materials with enhanced mechanical property, thermal conductivity and photo-thermal energy charging capacity. Energy Reports, 2020, 6: 2948–2955
34. Cai Z, Liu J, Zhou Y, et al. Flexible phase change materials with enhanced tensile strength, thermal conductivity and photo-thermal performance. Solar Energy Materials and Solar Cells, 2021, 219: 110728
35. Chen Y, Gao S, Liu C, et al. Preparation of PE-EPDM based phase change materials with great mechanical property, thermal conductivity and photo-thermal performance. Solar Energy Materials and Solar Cells, 2019, 200: 109988
36. Luo X, Hao B, Xiang H, et al. A novel phase change materials used for direct photothermal conversion and efficient thermal storage. Solar Energy Materials and Solar Cells, 2023, 251: 112142
37. Bai Y, Qiu W, Wang S. D-mannitol-based eutectic composite phase change materials with high thermal conductivity and solar-thermal conversion. International Journal of Energy Research, 2022, 46(11): 15722–15732
38. Gao H, Bing N, Xie H, et al. Energy harvesting and storage blocks based on 3D oriented expanded graphite and stearic acid with high thermal conductivity for solar thermal application. Energy, 2022, 254: 124198
39. Huo Y, Yan T, Chang X, et al. Expanded graphite@octadecanol composite phase change material with photothermal conversion interface. Solar Energy, 2023, 263: 111922
40. Wang S, Zhao X, Wang Z, et al. Micro-encapsulation of a low-melting-point alloy phase change material and its application in electronic thermal management. Journal of Cleaner Production, 2023, 417: 138058